Organic & Biomolecular Chemistry

Computational Investigation of Cycloadditions between Cyclopentadiene and Tropone-3,4-dimethylester.

Journal:	*Organic & Biomolecular Chemistry*
Manuscript ID	OB-ART-09-2022-001623.R1
Article Type:	Paper
Date Submitted by the Author:	27-Sep-2022
Complete List of Authors:	Milrod, Maya; Wesleyan University, Department of Chemistry Northrop, Brian; Wesleyan University, Department of Chemistry

ARTICLE

Computational Investigation of Cycloadditions between Cyclopentadiene and Tropone-3,4-dimethylester.

Received 00th January 20xx,
Accepted 00th January 20xx

DOI: 10.1039/x0xx00000x

Maya L. Milrod[a] and Brian H. Northrop*[a]

Thermally promoted cycloaddition reactions of tropone-3,4-dimethylester and cyclopentadiene have been investigated using density functional theory calculations at the M06-2X level and the CBS-QB3 method. The reaction shares several characteristics with previously investigated cycloadditions involving unsubstituted tropone and cyclopentadiene, however substitution of the tropone component with methyl esters results in lower transition state free energy barriers, greater thermodynamic driving forces, and a significant increase in the number of possible pericyclic reaction pathways. Eighteen possible [4+2], [6+4], or [8+2] cycloaddition products are possible and many of the initially formed cycloadducts can be interconverted through Cope or Claisen rearrangements. Of the many possible cycloaddition products only two are predicted to form: the *exo*-[6+4] product and one [4+2] product where the substituted tropone appears to be the diene. The two computationally predicted products are the same as the two that are observed experimentally, however computations indicate that both products result from ambimodal processes rather than single-step (monomodal) cycloaddition pathways.

Introduction

Beginning with their discovery in 1928[1] and accelerating after the development of orbital symmetry rules in 1969,[2] Diels-Alder [4+2] reactions have been the most thoroughly investigated class of cycloaddition reactions. The stereochemically-controlled formation of two new carbon-carbon bonds in a single concerted step makes [4+2] reactions a highly desired and useful synthetic transformation. Our research group has been particularly interested in the study of dynamically reversible [4+2] reactions, both from a theoretical point of view[3] and for their utility in dynamic covalent chemistry and as thermally labile protecting groups.[4,5] A small collection of Diels-Alder cycloaddition reactions have been shown to be reversible.[3,6-10] The majority of applications employing dynamic Diels-Alder reactions have focused on derivatives of furan and maleimide.[11] Within the context of dynamic covalent chemistry,[12-14] cycloaddition reactions have the desireable property of being 100% atom economical: all atoms contained in the reactants are present in the products. This can be especially desireable when applied to network materials such as self-healing and remouldable polymers.[11a-e] While there continues to be significant interest in the discovery and development of new reversible [4+2] cycloadditions, an alternative yet complementary approach would involve investigations of potentially reversible higher-order cycloadditions.[15,16]

In 1966 Itô and Cookson independently reported the [6+4] cycloaddition of tropone with cyclopentadiene.[17,18] This cycloaddition results in the *exo* adduct while the *endo* adduct is not formed on account of unfavorable secondary orbital interactions that were also predicted by orbital symmetry.[19] Several other thermal [6+4] cycloadditions have been reported[20-25] over the intervening 55 years including, more recently, metal[25,26] and organocatalytic examples.[27] Some [6+4] cycloadditions have even been shown to be catalyzed enzymatically in nature.[28-30] The details of [6+4] cycloadditions are, however, more complex than cycloadditions involving smaller π-systems. Some of this complexity is inherent to the fact that any [6+4] cycloaddition can have multiple competitive [4+2] processes. Furthermore, Caramella discovered[31] 20 years ago that even simple [4+2] reactions such as the dimerization of cyclopentadiene can involve bis-pericyclic transition states that are ambimodal, where a post-transition state bifurcation can result in the formation of multiple pericyclic products. Several groups have since investigated and reported examples of bis-pericyclic reactions.[32-39] Ambimodal processes appear to be especially prominent in higher-order cycloadditions such as [6+4] reactions. For example, a recent theoretical study by Houk et al. combined high accuracy DFT calculations (*w*B97X-D/def2-TZVP) with quasi-classical reaction dynamics to investigate the trajectories of a series of [6+4] cycloadditions and concluded that all *endo*-[6+4] cycloadditions are ambimodal.[40]

[a] *Wesleyan University, Department of Chemistry, 52 Lawn Ave., Middletown, CT 06459, USA. E-mail: bnorthrop@wesleyan.edu; Fax: +1 860 685-2211; Tel: +1 860 685-3987*

Electronic Supplementary Information (ESI) available: Full details and results of computational screen at the M06-2X/6-31G(d) level, calculated frontier orbital energies (HOMO and LUMO) of tropone, tropone diester **1** and cyclopentadiene, predicted product ratios from ambimodal reactions, Cartesian coordinates of all stationary points as well as their absolute enthalpies and free energies at both the M06-2X/6-31G(d) level and with the CBS-QB3 method. See DOI: 10.1039/x0xx00000x

Given the increased complexity and greater number of potentially competitive pericyclic processes involved in [6+4] cycloadditions any attempt to design dynamically reversible [6+4] reactions will benefit from computational modeling.[41] This is especially true when starting with substituted trienes and/or dienes, as substituents can break the symmetry of reactants and influence the relative kinetics and favorability of different pericyclic processes. Experimentally observed product ratios may not reveal the more complex details underlying their formation, i.e. what Houk et al. have referred to as "a web of hidden processes" that occur as part of the overall mechanism.[39] Mapping out all pericyclic processes computationally can provide considerable insight that can be used to understand experimental results and make actionable predictions. Toward this aim, we report a computational investigation of the pericyclic processes involved in thermally promoted reactions between tropone-3,4-dimethylester and cyclopentadiene (**1** and **2** in Scheme 1, respecitvely). Gleason et al. reported that heating **1** and **2** to reflux in toluene resulted in the formation of a mixture of *exo*-[6+4] product $\mathbf{3}_{exo}$ and *endo*-[4+2] product $\mathbf{4}_{endo}$ in a 1.5:1 ratio based on ^{1}H NMR analysis.[25] This experimental result provides a good model for computational studies of [6+4] cycloadditions involving a substituted triene component. Computations presented herein predict that multiple pericyclic processes, not simply the direct [4+2] and [6+4] reactions, are involved in the conversion of **1** and **2** into products $\mathbf{3}_{exo}$ and $\mathbf{4}_{endo}$. Ultimately our computational results suggest that the observed products are not predicted to form in a single step but, instead, transition state geometric parameters suggest that they follow from a mixture of ambimodal cycloaddition and sigmatropic pericyclic processes.

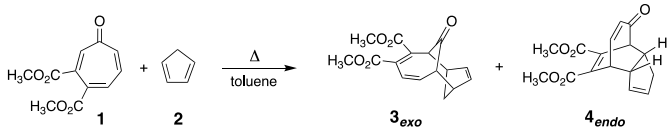

Scheme 1 Refluxing a toluene solution of tropone diester (**1**) and cyclopentadiene (**2**) was found to give [6+4] product $\mathbf{3}_{exo}$ and [4+2] product $\mathbf{4}_{endo}$

Results

The parent reaction of tropone with cyclopentadiene is known to give the *exo*-[6+4] product (Figure 1a). This result has been observed experimentally[17,18] and supported by several computational studies.[16,40] The transition state leading to the *endo*-[6+4] product has been calculated to be 3.3 kcal/mol less favored than the *exo*-[6+4] transition state (31.5 kcal/mol versus 28.2 kcal/mol, respectively) when modeled at the DLPNO-CCSD(T)/cc-pVQZ//*w*B97X-D/def2-TZVP level.[40] This difference is in line with the exclusive observation of the *exo* product. Despite the symmetry of both tropone and cyclopentadiene, the transition state leading to the observed [6+4] cycloadduct is asynchronous on account of stabilizing interactions between the tropone carbonyl oxygen atom and the π-system of cyclopentadiene. These interactions have been previously discussed by Houk et al.[40] and indicate that the transition state is really an ambimodal *exo*-[6+4]/[8+2] process that can also lead to the tricyclic product shown in Figure 1b. The [8+2] product is not as favored as the *exo*-[6+4] product, and a Claisen transition state enables the direct conversion of the [8+2] product to the more favored, and experimentally observed, *exo*-[6+4] product as indicated in Figure 1. The *endo*-[6+4] transition state is also ambimodal with the *exo*-[4+2] process shown in pathway **e** of Figure 1, as has also been observed previously. Other [4+2] reactions between tropone and cyclopentadiene are also possible, however they are not observed experimentally and have been shown computationally to be less favored.[40]

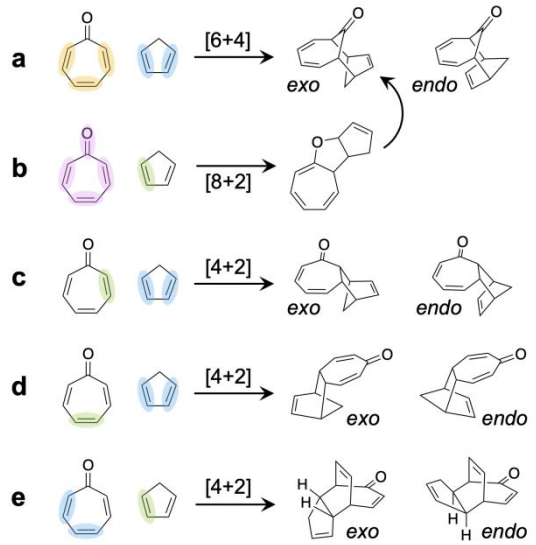

Fig. 1 Summary of the π-systems involved in [6+4]/[8+2] (**a**/**b**) and [4+2] (**c**-**e**) cycloaddition reactions between tropone and cyclopentadiene along with the chemical structures of their cycloaddition product. Reacting isolated alkenes are highlighted in green, dienes highlighted in blue, trienes highlighted in orange, and tetraenes in magenta.

A greater number of distinct cycloaddition reactions are possible upon reaction of tropone diester **1** and cyclopentadiene. Figure 2a highlights the π-systems involved in the [6+4] reactions that can take place involving all three C–C π-bonds of tropone diester **1** and the diene of cyclopentadiene. Two potential [8+2] cycloadditions can be envisioned and are highlighted in Figure 2b-c. While only six different [4+2] products are possible between unsubstituted tropone and cyclopentadiene given the C_{2v} symmetry of both reactants, fourteen unique [4+2] cycloaddition products are possible between **1** and **2** as highlighted in Figure 2d-2j (seven pathways each with *exo* and *endo* orientations of the reacting π-systems). Each possible cycloaddition can, in principle, progress with *exo* or *endo* orientations of the reacting π-systems. As will be seen, transition state geometries leading to several of the cycloadditions defined in Figure 2 are only subtly different. Furthermore, several of the cycloadditions between **1** and **2** are predicted to be ambimodal. Experimentally,[25] only two cycloaddition products are reported to form upon the thermal

reaction between **1** and **2**. Computationally, however, the picture is much more rich, complex, and interesting.

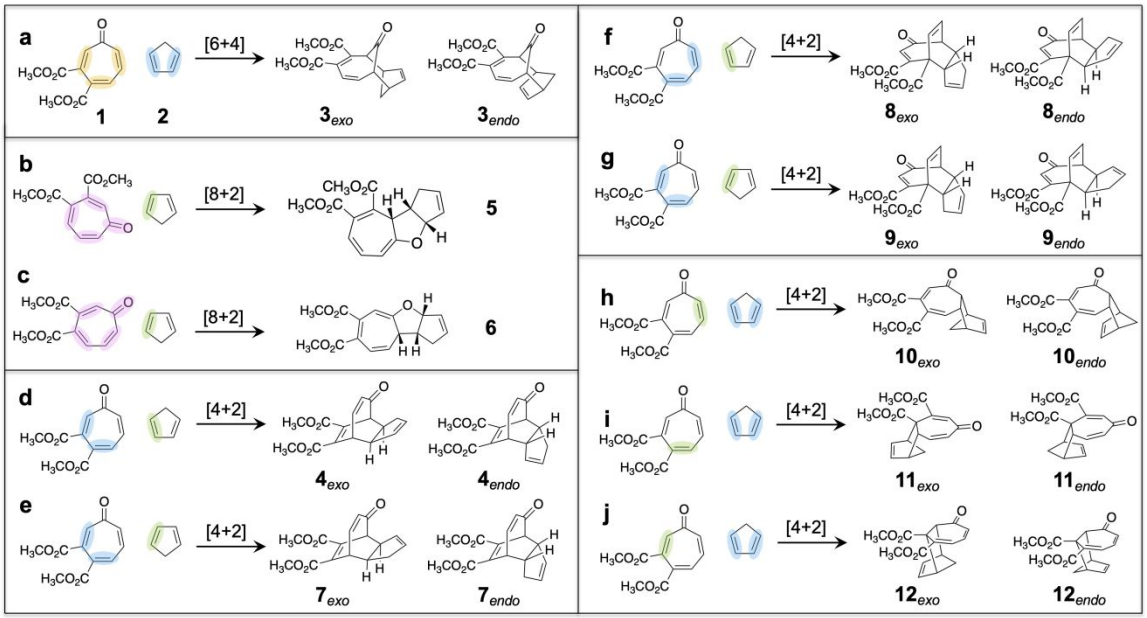

Fig 2. Summary of the π-systems involved in potential [6+4] (**a**), [8+2] (**b**-**c**(, and [4+2] (**d**-**j**) cycloaddition reactions between tropone diester **1** and cyclopentadiene (**2**), which are only numbered in reaction **a**. The coloring convention of Figure 1 is retained: reacting isolated alkenes are highlighted in green, dienes highlighted in blue, trienes highlighted in orange, and tetraenes in magenta.

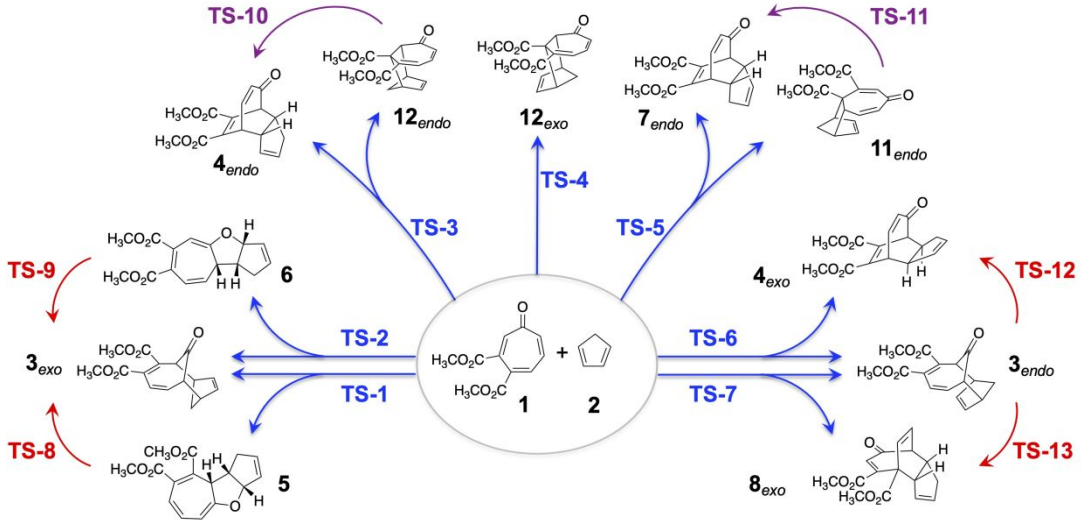

Scheme 2. Overview of the cycloaddition reactions between tropone diester **1** and cyclopentadiene that are predicted to be the most kinetically favored, i.e. lowest free energy barriers, as well as the sigmatropic processes that convert between several cycloaddition products. Cycloaddition processes (**TS-1** through **TS-7**) are highlighted in blue, Claisen rearrangements (**TS-8**, **TS-9**, **TS-12**, **TS-13**) are highlighted in red, and Cope rearrangements (**TS-10** and **TS-11**) are highlighted in purple. Transition states predicted to be ambimodal are indicated by branching arrows (note that this determination is made based on geometric analogies to known systems rather than molecular dynamics simulations). Sigmatropic rearrangements point in the direction of the more thermodynamically stable product. Cycloaddition transition states are arranged from lowest relative free energy (**TS-1**) to highest relative free energy (**TS-7**).

Given the large number of cycloaddition processes that are possible between tropone diester **1** and cyclopentadiene, an initial computational investigation at a modest level of computational theory, M06-2X/6-31G(d),[42] was undertaken to identify the processes that are most likely to lead to product formation. A complete summary of this initial investigation is provided in the Supporting Information (see section I, Figure S1, and Tables S1-S2 of the Supporting Information). Calculations at the M06-2X level of theory correctly identify products $\mathbf{3}_{exo}$ and $\mathbf{4}_{endo}$ as the most favored to form, as is observed experimentally.[25] However, the M06-2X/6-31G(d) calculations misidentify the [4+2] product $\mathbf{4}_{endo}$ as the major product and the [6+4] product $\mathbf{3}_{exo}$ as the minor product. Optimization of the transition states leading to these two products using the high-accuracy CBS-QB3 method[43] provides results that are

in better agreement with experiment, predicting $\mathbf{3}_{exo}$ to be major and $\mathbf{4}_{endo}$ to be minor. Given the better agreement with experiment,

Table 1. Calculated activation and reaction free energies[a] for all cycloaddition reactions and sigmatropic rearrangements summarized in Scheme 2.

Cycloaddition	TS-1	TS-2	TS-3	TS-4	TS-5	TS-6	TS-7
$\Delta G^{\ddagger}$	20.2	20.4	20.5	20.8	23.2	23.3	23.9

Rearrangement	TS-8	TS-9	TS-10	TS-11	TS-12	TS-13
$\Delta G^{\ddagger}$	23.5	23.8	18.3	23.1	23.2	21.4

Product	$\mathbf{3}_{exo}$	$\mathbf{3}_{endo}$	$\mathbf{4}_{exo}$	$\mathbf{4}_{endo}$	5	6	$\mathbf{7}_{endo}$	$\mathbf{8}_{exo}$	$\mathbf{11}_{endo}$	$\mathbf{12}_{exo}$	$\mathbf{12}_{endo}$
$\Delta G°$	-10.7	-6.6	-16.7	-18.6	-0.8	-4.3	-18.2	-14.1	-1.9	-2.1	-4.6

[a]All energies are calculated at the CBS-QB3 level of theory and given in kcal/mol.

additional calculations of potentially competitive cycloaddition reactions were carried out at the CBS-QB3 level. Overall, the seven cycloaddition pathways predicted to have the lowest free energy barriers at the M06-2X level were refined using CBS-QB3 calculations. Six of the seven transition states were found to be ambimodal, and sigmatropic rearrangements enable the interconversion between products that arise from the same ambimodal transition state. A summary of these seven pathways, the products they form, and sigmatropic rearrangements that convert between products is provided in Scheme 2. Relative transition state and reaction free energies (CBS-QB3) for all pericyclic reactions summarized in Scheme 2 are provided in Table 1.

Figure 3a outlines the pathways that convert tropone diester **1** and cyclopentadiene into observed *exo*-[6+4] product $\mathbf{3}_{exo}$. The two ester functionalities of tropone diester **1** break the symmetry of the molecule resulting in two different *exo*-[6+4] transition states shown as **TS-1** and **TS-2** in Figure 3b and 3c with key interatomic distances highlighted. These are the two lowest free energy cycloaddition transition states for the reaction between **1** and **2**. Where the two transition states differ is whether the newly developing C-C bond is more significantly formed at C2 of tropone diester **1**, as observed in **TS-1** (Figure 3b), or at C7 of tropone diester **1**, as observed in **TS-2** (Figure 3c). These shorter C-C distances are highlighted by black dashed bonds in **TS-1** and **TS-2**. Both transition states display additional bond forming/breaking interactions that are highlighted in green for C-C interactions and red for C-O interactions. The observation of these longer, competing partial bonding interactions indicates that both **TS-1** and **TS-2** exhibit ambimodal character, as has also been observed for the parent reaction between unsubstituted tropone and cyclopentadiene.[40] In this case, **TS-1** and **TS-2** are ambimodal *exo*-[6+4]/[8+2] processes that can both lead to [6+4] product $\mathbf{3}_{exo}$, however only **TS-1** can also form [8+2] isomer **5** while only **TS-2** leads to [8+2] isomer **6**. The relative free energy barriers of **TS-1** and **TS-2** are predicted to be very similar at $\Delta G^{\ddagger}$ = 20.2 and 20.4 kcal/mol, respectively. Formation of the *exo*-[6+4] product $\mathbf{3}_{exo}$ is thermodynamically favored with a relative free energy of $\Delta G°$ = -10.7 kcal/mol versus $\Delta G°$ = -0.8 and -4.3 kcal/mol for [8+2] products **5** and **6**, respectively. Each [8+2] product, however, can be converted into $\mathbf{3}_{exo}$ by a Claisen rearrangement: [8+2] isomer **5** is converted into $\mathbf{3}_{exo}$ by **TS-8** (Figure 3d) while [8+2] isomer **6** is converted into $\mathbf{3}_{exo}$ via **TS-9** (Figure 3e). Claisen transition states **TS-8** and **TS-9** are found to be 3.3 and 3.4 kcal/mol higher energy than their associated cycloaddition transition states **TS-1** and **TS-2**, which is similar to earlier computational analysis of Houk et al. who found the Claisen transition state involving unsubstituted tropone and cyclopentadiene to be 3.2 kcal/mol higher energy than the ambimodal [6+4]/[8+2] transition state.[40]

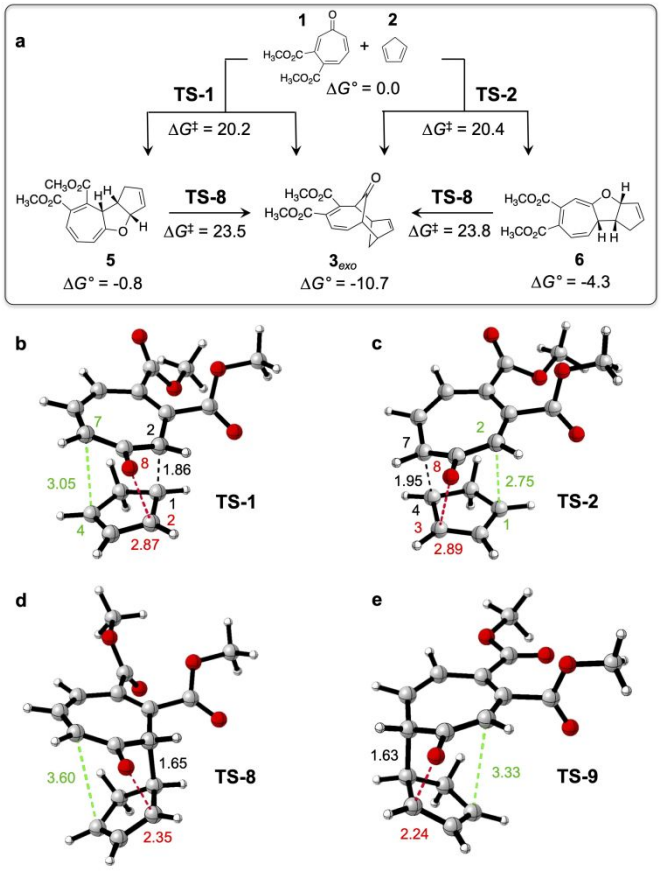

Fig 3 (**a**) Reaction pathways outlining the conversion of tropone diester **1** and cyclopentadiene into observed major product $\mathbf{3}_{exo}$. Calculated cycloaddition transition structures **TS-1** and **TS-2** are shown in (**b**) and (**c**), respectively, while Claisen rearrangement

transition structures **TS-8** and **TS-9** are shown in (**d**) and (**e**), respectively. Relative reaction and transition state free energies are given in kcal/mol and interatomic distances are given in Å.

Houk et al. have demonstrated that product ratios of an ambimodal process can be related to differences in interatomic distances of competing bond forming/breaking interactions of the ambimodal transition structure.[44] This analysis can be applied to transition states **TS-1** and **TS-2** to approximate which cycloaddition product, [6+4] or [8+2], is favored by each transition state. In **TS-1**, carbon atoms C2 of tropone diester **1** and C1 of cyclopentadiene are separated by 1.86 Å, which is the shortest of the three bond forming/bond breaking interactions highlighted in Figure 3b and therefore the "dominant" bond that is formed regardless of whether bifurcation leads to the [6+4] or [8+2] product. C-C bond formation between C7 of tropone diester **1** and C4 of cyclopentadiene, highlighted in green, results in the *exo*-[6+4] product while formation of a C-O bond between O8 of **1** and C2 of **2**, highlighted in red, gives the [8+2] product. Computations predict O8-C2 to be more fully formed in the transition structure with a separation of 2.87 Å relative to C7-C4, which are separated by 3.05 Å. This difference of 0.27 Å between the developing O-C and C-C bonds predicts that the [8+2] product **5** is favored to form in a 76:24 ratio relative to *exo*-[6+4] product $\mathbf{3}_{exo}$. As can be seen in Table 1, *exo*-[6+4] product $\mathbf{3}_{exo}$ is predicted to be -9.9 kcal/mol more stable than [8+2] product **5** and, as shown in Scheme 2 and Figure 3, product **5** can be converted into product $\mathbf{3}_{exo}$ by Claisen transition state **TS-8**. Calculations therefore suggest that the most favored cycloaddition between tropone diester **1** and cyclopentadiene is predicted to lead to an approximate 3:1 ratio of **5** and $\mathbf{3}_{exo}$, however unobserved [8+2] product **5** is subsequently converted into observed product $\mathbf{3}_{exo}$ by either sigmatropic rearrangement or retrocyclization. The computationally predicted [8+2]/*exo*-[6+4] favorability is reversed in **TS-2** where the C2-C1 bond highlighted in green is more fully developed at 2.75 Å relative to the O8-C3 bond highlighted in red, which is 2.89 Å. Houk's model predicts *exo*-[6+4] product $\mathbf{3}_{exo}$ is favored by an approximate ratio of 87:13 relative to [8+2] product **6**. While [8+2] product **6** is more favored than isomer **5** ($\Delta G°$ of -4.3 versus -0.8 kcal/mol), conversion of minor product **6** into observed product $\mathbf{3}_{exo}$ via Claisen transition state **TS-9** is exergonic by -6.3 kcal/mol. Overall, the two lowest free energy transition states **TS-1** and **TS-2** both lead to the observed major product $\mathbf{3}_{exo}$ via either direct [6+4] cycloaddition or [8+2] cycloaddition followed by rearrangement.

Multiple [4+2] cycloaddition processes involving tropone diester **1** and cyclopentadiene are possible as shown in Figure 2. Initial M06-2X screening of all cycloaddition processes narrowed the scope of this CBS-QB3 study to the five [4+2] cycloadditions **TS-3** through **TS-7** shown in Scheme 2; seven additional cycloaddition processes were ruled out as non-competitive toward product formation (see Supporting Information section I). Of all possible [4+2] cycloadditions those involving cyclopentadiene as the diene and the C2-C3 alkene of tropone diester **1** as the dienophile, i.e. **TS-3** and **TS-4** shown in Figure 4, were found to be the most favorable. Where the two transition states differ is whether the π-system of cyclopentaciene is positioned under the π-system of tropone diester **1** (*endo*, **TS-3**) or out from under the π-system of **1** (*exo*, **TS-4**). **TS-3** has a calculated energy barrier of $\Delta G^{‡}$ = 20.5 kcal/mol, which is only 0.3 and 0.1 kcal/mol higher energy than **TS-1** and **TS-2**, respectively. **TS-3** is ambimodal and bifurcates to give experimentally observed product $\mathbf{4}_{endo}$ as well as $\mathbf{12}_{endo}$. Looking at the structure of **TS-3** in Figure 4b, the forming C2–C4 bond is the shortest at 1.91 Å and will be formed regardless of whether $\mathbf{4}_{endo}$ or $\mathbf{12}_{endo}$ is the major product. The forming C5-C3 bond of **TS-3**, which leads to product $\mathbf{4}_{endo}$, is slightly shorter (3.20 Å) than the forming C3-C1 bond (3.24 Å) that leads to product $\mathbf{12}_{endo}$. This difference of 0.04 Å suggests that $\mathbf{4}_{endo}$ will be more likely to form via **TS-3** than $\mathbf{12}_{endo}$ with a predicted ratio of 3:2. Product $\mathbf{12}_{endo}$, however, was not observed by Gleason et al.[25] while product $\mathbf{4}_{endo}$ was. This is explained by the fact that $\mathbf{12}_{endo}$ is able to undergo a Cope rearrangement (**TS-10**, Figure 4d) to give $\mathbf{4}_{endo}$ with a predicted relative free energy barrier of $\Delta G^{‡}$ = 18.3 kcal/mol. The Cope rearrangement from $\mathbf{12}_{endo}$ to the experimentally observed $\mathbf{4}_{endo}$ product is exergonic by 16.5 kcal/mol. The observation that the C3-C1 bond of **TS-10** is significantly shorter (2.51 Å) than the C5-C3 bond (3.35 Å) indicates that the Cope transition state more closely resembles the structure of $\mathbf{12}_{endo}$, which is indicative of an early transition state in accord with the Hammond Postulate and further supports observation that the rearrangement of $\mathbf{12}_{endo}$ to $\mathbf{4}_{endo}$ exothermic.

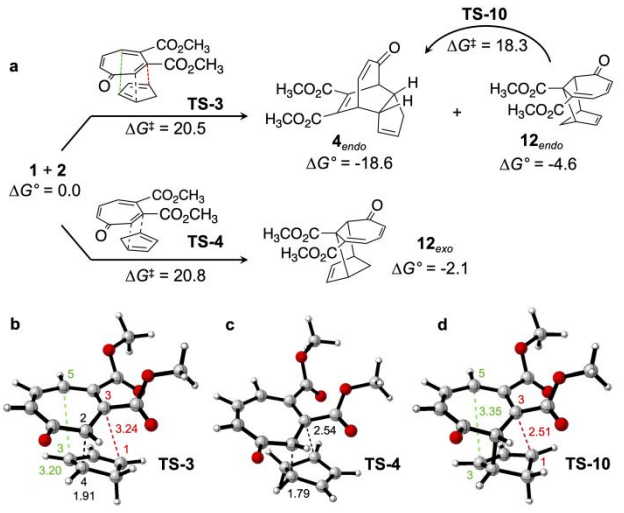

Fig 4 (**a**) Reaction of cyclopentadiene with the C2-C3 alkene of tropone diester **1** along *endo* (top) and *exo* (bottom) pathways to give cycloaddition products $\mathbf{4}_{endo}$, $\mathbf{4}_{exo}$, and $\mathbf{12}_{endo}$. Calculated cycloaddition transition structures **TS-3** and **TS-4** are shown in (**b**) and (**c**), respectively, while Cope transition structure **TS-10** is shown in (**d**). Relative energies are given in kcal/mol and interatomic distances are given in Å.

TS-4 (Figure 4c) leads to product $\mathbf{12}_{exo}$ and has a calculated free energy barrier of $\Delta G^{\ddagger}$ = 20.8 kcal/mol. It is not ambimodal and cannot undergo a Cope rearrangement to an alternative cycloaddition product. While computations predict **TS-4** to be only 0.7 kcal/mol higher energy than the most favored transition state **TS-1**, the [4+2] product $\mathbf{12}_{exo}$ is not observed experimentally. We suggest that formation of $\mathbf{12}_{exo}$ is reversible given its low thermodynamic driving force of $\Delta G°$ = -2.1 kcal/mol. Both experimentally observed products $\mathbf{3}_{exo}$ and $\mathbf{4}_{endo}$ are more exergonic relative to reactants **1** and **2** (-10.7 and -18.6 kcal/mol, respectively) and are therefore both kinetically and thermodynamically favored.

Three additional cycloaddition processes were studied at the CBS-QB3 level in an effort to ensure all competitive cycloadditions were considered and evaluated. The calculated structures of transition states **TS-5**, **TS-6**, and **TS-7** are shown in Figure 5. All three cycloadditions are ambimodal as indicated earlier in Scheme 2. None of the three cycloadditions shown in Figure 5 would be expected to lead to products given that they are all at least 3.0 kcal/mol less favored than *exo*-[6+4]/[8+2] transition state **TS-1**. Their structures and relative energetics are still worth evaluating, however, as they help provide additional insight into the effects of the two withdrawing methyl ester functionalities of tropone diester **1**.

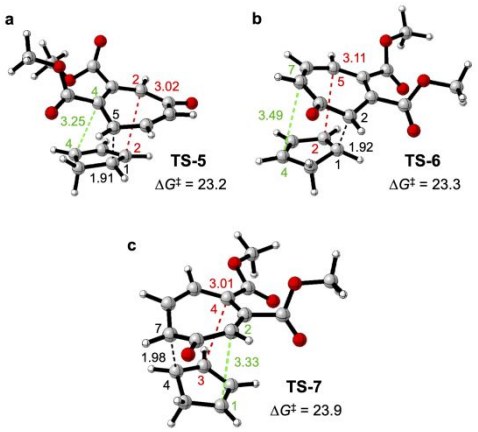

Fig 5 Calculated cycloaddition transition structures **TS-5** (**a**), **TS-6** (**b**), and **TS-7** (**c**). Transition state free energies are given relative to tropone diester **1** and cyclopentadiene starting materials and given in kcal/mol. Interatomic distances are given in Å.

TS-5 shown in Figure 5a leads to [4+2] cycloaddition products $\mathbf{7}_{endo}$ and $\mathbf{11}_{endo}$. The shortest bond forming/breaking interaction in **TS-5** is between C5 of tropone diester **1** and C1 of cyclopentadiene. The C2-C2 interatomic distance, which leads to product $\mathbf{7}_{endo}$, is shorter than the C4-C4 interatomic distance that leads to product $\mathbf{11}_{endo}$: 3.02 versus 3.24 Å. [4+2] product $\mathbf{7}_{endo}$ is therefore predicted to be more likely to form via **TS-5** in a 9:1 ratio over $\mathbf{11}_{endo}$. Any quantities of $\mathbf{11}_{endo}$ that might form would be expected to convert to $\mathbf{7}_{endo}$ via Cope transition state **TS-11** ($\Delta G^{\ddagger}$ = 23.1 kcal/mol) given that $\mathbf{7}_{endo}$ is predicted to be more stable by 16.3 kcal/mol.

Just as two different ambimodal *exo*-[6+4]/[8+2]cycloaddition transition states are able to give produc $\mathbf{3}_{exo}$, two ambimodal *endo*-[6+4]/[4+2] cycloaddition transition states are able to produce $\mathbf{3}_{endo}$. The two calculated *endo*-[6+4]/[4+2] transition structures **TS-6** and **TS-7** are shown in Figure 5b and 5c, respectively. The ambimodal processes differ by which C-C bond is more fully formed (i.e. shorter) in the transition state: the one proximal to the esters of tropone diester **1**, as in **TS-6**, or the C-C bond distal to the esters, as seen in **TS-7**. In both cases the C-C bond leading to an *exo*-[4+2] product is shorter than the C-C bond leading to the *endo*-[6+4] product: 3.11 versus 3.49 Å in **TS-6** and 3.01 versus 3.33 Å in **TS-7**. These differences suggest that [4+2] adducts $\mathbf{4}_{exo}$ and $\mathbf{8}_{exo}$ will be the major product (≥95%) of ambimodal transition states **TS-6** and **TS-7**, respectively, while the *endo*-[6+4] $\mathbf{3}_{endo}$ will be minor. The minor [6+4] product $\mathbf{3}_{endo}$ is also predicted to be less thermodynamically favorable than either of the [4+2] products, with calculated reaction free energies of $\Delta G°$ = -6.6, -16.7, and -14.1 kcal/mol for products $\mathbf{3}_{endo}$, $\mathbf{4}_{exo}$, and $\mathbf{8}_{exo}$, respectively. The less favored $\mathbf{3}_{endo}$ product can, however, be converted into [4+2] products $\mathbf{4}_{exo}$ or $\mathbf{8}_{exo}$ through Cope rearrangements **TS-12** or **TS-13**, respectively. Overall, these results are consistent with those found previously for the *endo*-[6+4] reaction of unsubstituted tropone and cyclopentadiene,[40] namely that (i) the transition state is ambimodal with a [4+2] process, (ii) the *exo* transition state is more favored, and (iii) a Cope transition state converts between the [6+4] and [4+2] products with the [4+2] product being thermodynanmically favored.

The free energies of transition states **TS-1** through **TS-7** can be used to predict their approximate contributions to product formation. Given the relative free energy differences between the seven different transition states, transition state theory (TST)[45] would predict their contributions to product formation to be: **TS-1** (39.1%), **TS-2** (25.6%), **TS-3** (21.3%), **TS-4** (13.5%), **TS-5** (0.2%), **TS-6** (0.2%), and **TS-7** (<0.1%). These results suggest that extending the CBS-QB3 investigation to include all remaining, less favored cycloaddition transition states would be unnecessary given that transition states **TS-1** through **TS-4** are predicted to contribute to >99.5% of product formation. Furthermore, as discussed above, the formation of $\mathbf{12}_{exo}$ via **TS-4** is predicted to be reversible given the low thermodynamic driving force of the reaction and the fact that $\mathbf{12}_{exo}$ was not observed experimentally by Gleason et al. Under the assumption that the formation of $\mathbf{12}_{exo}$ is indeed reversible then any quantities of $\mathbf{12}_{exo}$ formed will cycle over to the more thermodynamically favorable and kinetically accessible products formed via transition states **TS-1**, **TS-2**, and **TS-3**. When considering only these three lowest free energy transition states, TST predicts **TS-1** and **TS-2**, which lead to the formation of $\mathbf{3}_{exo}$, will account for 45.4% and 29.8% of product formation while **TS-3**, which leads to $\mathbf{4}_{endo}$, will account for 24.8% of product formation. CBS-QB3 calculations therefore predict $\mathbf{3}_{exo}$ to be the major product that is formed in a 3:1 ratio relative to the minor product $\mathbf{4}_{endo}$. This is in general agreement, though

slightly higher, than the experimentally determined ratio of $\mathbf{3}_{exo}$ to $\mathbf{4}_{endo}$, which was found to be 1.5:1.

Discussion

The results above detail the pericyclic pathways that lead from tropone diester **1** and cyclopentadiene to experimentally observed [6+4] product $\mathbf{3}_{exo}$ and [4+2] product $\mathbf{4}_{endo}$. As noted, similar pericyclic processes have been investigated previously for tropone and cyclopentadiene. Even prior to any computational or experimental investigation, it would be apparent that the two ester groups of tropone diester **1** will have the effects of desymmetrizing the molecule and increasing its electrophilicity relative to parent, unsubstituted tropone. Developing a thorough understanding of the role(s) of substituents in competitive higher-order cycloaddition reactions will be necessary in order to explain experimental outcomes, make predictions, and, ideally, design new dynamically reversible cycloaddition reactions. Toward that aim it is important to discuss the impact of diester substitution in **1** relative to unsubstituted tropone.

In pericyclic reactions involving cyclopentadiene and either unsubstituted tropone or tropone diester **1**, the tropone is more electron poor and behaves as the electrophilic component while cyclopentadiene is the more electron rich nucleophilic component. CBS-QB3 calculations predict that the addition of methyl ester substituents at the 3- and 4-positions of tropone lowers the LUMO of **1** by 0.4 eV relative to unsubstituted tropone (see Supporting Information). Therefore, it is unsurprising that the impact of diester substitution is to lower the free energy barrier and increase the exergonicity of ~~every~~ cycloaddition reactions between cyclopentadiene and tropone **1** relative to the analogous cycloadditions between cyclopentadiene and unsubstituted tropone. For example, *exo*-[6+4]/[8+2] transition states **TS-1** and **TS-2** (Figure 3) have ~~a~~ free energy barriers that are 8.0 and 7.8 kcal/mol lower than the corresponding ambimodal transition state involving unsubstituted tropone investigated previously[39] ($\Delta G^{\ddagger}$ of 20.2 and 20.4 versus 28.2 kcal/mol). Structurally, the influence of diester substitution can be seen in bond distances of forming/breaking bonds in **TS-1** and **TS-2**. In both transition states the oxygen-carbon distances are similar at 2.87 Å in **TS-1** and 2.89 Å in **TS-2** (Figure 3b and c, red dashed lines). Where the two transition states differ is in their C2-C1 and C7-C4 bond distances. In particular, comparisons across **TS-1** and **TS-2** reveal that bond forming/breaking interactions involving C2 of tropone diester **1**, i.e. the tropone carbon closest to the withdrawing ester groups, are shorter. For example, the shortest developing bond in **TS-1** is between C2-C1 (i.e. it does involve C2 of tropone diester **1**) and is calculated to be 1.86 Å while the shortest developing bond of **TS-2** is between C7-C4 and found to be 0.09 Å longer at 1.95 Å. Comparing the other bond involved in *exo*-[6+4] product formation (highlighted by a dashed green line in Figures 3b and 3c) shows an even larger difference that favors shorter interatomic distances involving C2 of **1**. The C7-C4 distance in **TS-1** is 3.05 Å while the C2-C1 distance in **TS-2** is 0.3 Å shorter at 2.75 Å. These structural differences suggest the withdrawing effects of diester substitution increase the reactivity at carbon 2 of tropone diester **1**. Lastly, the formation of [6+4] product $\mathbf{3}_{exo}$ is predicted to be 1.5 kcal/mol more exergonic than in the unsubstituted case.

The only cycloaddition reactions found to be competitive with *exo*-[6+4]/[8+2] processes **TS-1** and **TS-2** were those that involve reaction at the C2-C3 alkene of tropone diester **1**, i.e. **TS-3** and **TS-4** (Figure 4). This observation suggests that the C2-C3 alkene is the most reactive dienophile of tropone diester **1**. The C2-C3 alkene is directly conjugated to the withdrawing methyl ester at carbon 3 and the tropone carbonyl, which likely explains its greater reactivity. When examining the structures of transition states **TS-3** and **TS-4** it is notable that, again, bond forming/breaking interactions that involve the C2 carbon of tropone diester **1** are the shortest at 1.91 and 1.79 Å, respectively. **TS-3** has a lower relative free energy than **TS-4** because of bond forming/breaking interactions between C5 of tropone diester **1** and C3 of cyclopentadiene that also account for the ambimodal nature of **TS-3**. This C5-C3 interaction is stronger than the C3-C1 interaction, based on interatomic distances, and leads to the formation of experimentally observed product $\mathbf{4}_{endo}$. The formation and favorability of $\mathbf{4}_{endo}$ is noteworthy because it represents an inverse electron demand process where electron poor tropone diester **1** reacts as the diene and comparatively electron rich cyclopentadiene is the dienophile. We suggest the relatively low free energy barrier ($\Delta G^{\ddagger}$ = 20.5 kcal/mol) of this inverse electron demand cycloaddition is enabled by two factors: (i) direct conjugation of methyl esters with both terminal ends of the diene, rendering it especially electron poor and therefore reactive, and (ii) the additional stabilization afforded by its ambimodal nature, wherein **TS-3** is a blend of the inverse electron demand cycloaddition leading to $\mathbf{4}_{endo}$ and the most favored [4+2] cycloaddition involving cyclopentadiene as the diene reacting with the most reactive C2-C3 dienophile of tropone diester **1**.

Cycloaddition transition states **TS-5**, **TS-6**, and **TS-7** (Figure 5) also involve bond forming/breaking interactions at C2 of tropone diester **1**, further highlighting the increased reactivity at that position. All three transition states, however, are sufficiently less stable than transition states **TS-1** through **TS-4** that they are predicted to account for <0.5% of product formation. Still, their structures further highlight the impact of methyl ester substitution at positions 3 and 4 of tropone. Transition state **TS-5**, for example, represents another example of an inverse electron demand Diels-Alder reaction leading to the formation of $\mathbf{7}_{endo}$. The transition state involves the same diene of tropone diester **1** that is withdrawn by both methyl ester groups, however it is 2.5 kcal/mol less stable than **TS-3** that involves the same diene. The higher free energy of **TS-5** is believed to be because the other cycloaddition product of the ambimodal transition state is $\mathbf{11}_{endo}$, which involves the C4-C5

alkene of tropone diester **1** as the dienophile. The C4-C5 alkene is less reactive than the C2-C3 alkene given that it is directly conjugated to only one methyl ester withdrawing group.

Endo-[6+4]/[4+2] transition states **TS-6** and **TS-7** further reinforce observations regarding the impact of diester substitution noted above. Both transition states are ambimodal and lead to the formation of [6+4] product $\mathbf{3}_{endo}$ along with an inverse electron demand [4+2] product where cyclopentadiene is the dienophile and tropone diester **1** is the diene. Despite these similarities, CBS-QB3 computations predict **TS-6** to be 0.6 kcal/mol more stable than **TS-7**. The primary reasons for the greater stability of **TS-6** are twofold and in line with earlier observations. In particular, the shortest bond forming/breaking interaction of **TS-6** involves the highly reactive C2 of tropone diester **1** whereas the shortest bond forming/breaking interaction of **TS-7** does not. Additionally, the inverse electron demand component of **TS-6**, which leads to product $\mathbf{4}_{exo}$, involves the more reactive diene of tropone diester **1** (C2-C3 and C4-C5). The inverse electron demand component of **TS-7** involves a less reactive diene composed of the C4-C5 and C6-C7 alkenes of tropone diester **1**.

Conclusions

While only one example, this study of cycloaddition reactions between tropone diester **1** and ~~2~~ cyclopentadiene suggests that one means of understanding and tuning the reactivity of higher-order, competitive cycloaddition reactions is to begin with a computational evaluation of where and how significantly a substituent(s) increases or decreases the electrophilicity or nucleophilicity of reacting partners overall (e.g. tropone diester **1** is more electrophilic than unsubstituted tropone) as well as individual π-components within each reactant (e.g. the C2-C3 alkene is the most reactive of **1**). In the current study, ambimodal processes ~~a~~appear to be kinetically favored over nearly all single trajectory cycloadditions, likely on account of additional stabilizing interactions in their transition states. Further computational investigations of similarly substituted systems will be necessary to see if this is a general observation or limited to the current system. Steric factors may also come into play in some systems, however electronic influences appear to be consequential in most cases. Computations will continue to be an invaluable mainstay of this kind of research for not only their predictive value but, significantly, because of the complex and often interconverting web of pericyclic processes that occur "behind the scenes," hidden from experimental observation. Future work along these lines aims to design higher-order cycloaddition reactions that are dynamically reversible while continuing to explore the role of ambimodal processes in higher-order cycloaddition reactions.

Computational Details

Theoretical calculations were carried out using the program Gaussian16 along with the GaussView6 graphical user interface.[46] Initial structures were constructed within GaussView6 and a conformational search was carried out at the M06-2X/6-31G(d)[42,47] level of theory by scanning any bonds that could rotate freely, e.g. the methyl ester substituents of substituted tropone **1**. Approximate global minima from these conformational searches were then optimized to full convergence at the M06-2X/6-31G(d) level. Thermal and vibrational analysis was used to confirm minima as having only real vibrational frequencies. Cycloaddition and sigmatropic (Cope and Claisen) transition states were located following extensive searches of the potential energy surface along internal coordinates corresponding to bond breaking and bond formation. Approximate transition structures were then subjected to a Berny optimization and confirmed as saddle points by the presence of a single imaginary vibrational frequency. Forward and reverse internal reaction coordinate (IRC) calculations,[48] followed by geometry optimizations, were used to confirm relationships between reactants, products, and transition states. Ambimodal transition states were distinguished as having (i) a single breaking/forming bond that is common to both pericyclic products and is relatively well developed at ~1.8-2.2 Å, and (ii) two additional breaking/forming bonds that distinguish the two pericyclic products that are longer at ~2.8-3.3 Å. Atom trajectories in the single imaginary vibrational mode and pyramidalization of conjugated carbon atoms away from planarity also helped identify ambimodal transition states, however, it is important to note that molecular dynamics trajectories were not investigated in the current study. To evaluate the possible involvement of diradical species, all M06-2X wavefunctions were checked for stability and all wavefunctions were found to be stable under the perturbations considered. The influence of solvent was also investigated using a CPCM implicit solvent model[49] for toluene, the solvent used experimentally by Gleason.[25] Solvation in toluene did not substantively change the reaction energetics (see Supplementary Information section Ie). The CBS-QB3 compound method[43] was used to refine the reaction energetics of the seven most favored cycloaddition pathways as shown in Scheme 2. Optimized M06-2X/6-31G(d) geometries of all reactants, transition states, and products along these seven pathways and the sigmatropic rearrangements that convert between products were used as inputs for subsequent CBS-QB3 calculations. All stationary point optimizations were performed in the gas phase at 298.15 K and 1.0 atm pressure, and all relative free energies in this manuscript are reported in kcal/mol. The program CLYView 2.0[50] was used to generate 3D representations of stationary points presented throughout the manuscript.

Author Contributions

M. L. M Investigation, Formal Analysis, Writing – review & editing. B. H. N. Conceptualization, Methodology, Supervision, Investigation, Formal Analysis, Writing – original draft, review, & editing.

Conflicts of interest

There are no conflicts to declare.

Acknowledgements

The authors gratefully acknowledge Wesleyan University for computer time supported by the NSF under grant number CNS-0619508 and Prof. James Gleason for helpful discussions.

Notes and references

1 O. Diels, K. Alder, Synthesen in der hydroaromatischen Reihe, I. *Justus Liebigs Annalen der Chemie*, **1928**, *460*, 98-122.
2 R.B. Woodward, R. Hoffmann, The Conservation of Orbital Symmetry. *Angew. Chem., Int. Ed. Engl.* **1969**, *8*, 781-853.
3 R. C. Boutelle, B. H. Northrop, Substituent Effects on the Reversibility of Furan-Maleimide Cycloadditions. *J. Org. Chem.* **2011**, *76*, 7994-8002.
4 R. M. Stolz, B. H. Northrop, Experimental and Theoretical Studies of Selective Thiol-Ene and Thiol-Yne Click Reactions Involving *N*-Substituted Maleimides. *J. Org. Chem.* **2013**, *78*, 8105-8116.
5 S. H. Frayne, R. M. Stolz, B. H. Northrop, Dendritic Architectures by Orthogonal Thiol-Maleimide "Click" and Furan-Maleimide Dynamic Covalent Chemistries. *Org. Biomol. Chem.* **2019**, *17*, 7878-7883.
6 P. J. Boul, P. Reutenauer, J.-M. Lehn, Reversible Diels-Alder Reactions for the Generation of Dynamic Combinatorial Libraries. *Org. Lett.* **2005**, *7*, 15-18.
7 B. Masci, S. Pasquale, P. Thuery, P. Supramolecular Control of a Fast and Reversible Diels-Alder Reaction. *Org. Lett.* **2008**, *10*, 4835-4838.
8 P. Reutenauer, P. J. Boul, J.-M. Lehn, Dynamic Diels-Alder Reactions of 9,10-Dimethylanthracene: Reversible Adduct Formation, Dynamic Exchange Processes and Thermal Fluorescence Modulation. *Eur. J. Org. Chem.* **2009**, *11*, 1691-1697.
9 A. L. Widstrom, B. J. Lear, Structural and Solvent Control Over Activation Parameters for a Pair of Retro Diels-Alder Reactions. *Scientific Reports* **2019**, *9*, 18267.
10 K. Kawai, K. Ikeda, A. Sato, A. Kabasawa, M. Kojima, K. Kokado, A. Kakugo, K. Sada, T. Yoshino, S. Matsunaga, 1,2-Disubstituted 1,2-dihydro-1,2,4,5-tetrazine-3,6-dione as a Dynamic Covalent Bonding Unit at Room Temperature. *J. Am. Chem. Soc.* **2022**, *144*, 1370-1379.
11 See, for example: (a) X. Chen. M. A. Dam, K. Ono, A. Mal, H. Shen, S. R. Nutt, K. Sheran, F. Wudl, Thermally Re-mendable Cross-Linked Polymeric Material. *Science* **2002**, *295*, 1698-1702. (b) B. J. Adzima, H. A. Aguirre, C. J. Kloxin, T. F. Scott, C. N. Bowman, Rheological and Chemical Analysis of Reverse Gelation in a Covalently Cross-Linked Diels-Alder Polymer Network. *Macromolecules* **2008**, *41*, 9112-9117. (c) G. A. Appuhamillage, J. C. Reagan, S. Khorsandi, J. R. Davidson, W. Voit, R. A. Smaldone, 3D Printed Remendable Polylactic Acid Blends with Uniform Mechanical Strength Enabled by a Dynamic Diels-Alder Reaction. *Polym. Chem.* **2017**, *8*, 2087-2092. (d) B. Strachota, A. Morand, J. Dybal, L. Matejka, Control of Gelation and Properties of Reversible Diels-Alder Networks: Design of a Self-Healing Network. *Polymers* **2019**, 11, 930. (e) K.-K. Tremblay-Parrado, C. Bordin, S. Nicholls, B. Heinrich, B. Donnio, L. Averous, Renewable and Responsive Cross-Linked Systems Based on Polyurethane Backbones from Clickable Biobased Bismaleimide Architecture. *Macromolecules* **2020**, *53*, 5869-5880. (f) X. Hu, T. Zeng, C. C. Husic, M. J. Robb, Mechanically Triggered Release of Functionally Diverse Molecular Payloads from Masked 2-Furylcarbinol Derivatives. *ACS Cent. Sci.* **2021**, *7*, 1216-1224.
12 S. J. Rowan, S. J. Cantrill, G. R. L. Cousins, J. K. M. Sanders, J. F. Stoddart, Dynamic Covalent Chemistry. *Angew. Chem., Int. Ed.* **2002**, *41*, 898-952.
13 Y. Jin, C. Yu, R. J. Denman, W. Zhang, Recent Advances in Dynamic Covalent Chemistry. *Chem. Soc. Rev.* **2013**, *42*, 6634-6654.
14 G. M. Scheutz, J. J. Lessard, M. B. Sims, B. S. Sumerlin, Adaptable Crosslinks in Polymeric Materials: Resolving the Intersection of Thermoplastics and Thermosets. *J. Am. Chem. Soc.* **2019**, *141*, 16181-16196.
15 T. A. Palazzo, R. Mose, K. A. Jørgensen, Cycloaddition Reactions: Why is it so Challenging to Move from Six to Ten Electrons? *Angew. Chem., Int. Ed.* **2017**, *56*, 10033-10038.
16 D. McLeod, M. K. Thøgersen, N. I. Jessen, K. A. Jørgensen, C. S. Jamieson, X.-S. Xue, K N. Houk, F. Liu, R. Roffmann, Expanding the Frontiers of Higher-Order Cycloadditions. *Acc. Chem. Res.* **2019**, *52*, 3488-3501.
17 S. Itô, Y. Fujise, T. Okuda, Y. Inoue, Reaction of Tropone with Cyclopentadiene. *Bull. Chem. Soc. Jpn.* **1966**, *39*, 1351.
18 R. C. Cookson, B. V. Drake, J. Hudec, A. Morrison, The Adduct of Tropone and Cyclopentadiene: A New Type of Cyclic Reaction. *Chem. Commun.* **1966**, 15-16.
19 R. Hoffmann, R. B. Woodward, Orbital Symmetries and Endo-Exo Relationships in Concerted Cycloaddition Reactions. *J. Am. Chem. Soc.* **1965**, *87*, 4388-4389.
20 K. N. Houk, R. B. Woodward, Cycloaddition Reactions of Cycloheptatriene and 2,5-Dimethyl-3,4-diphenylcyclopentadienone. *J. Am. Chem. Soc.* **1970**, *92*, 4143-4145.
21 K. N. Houk, R. B. Woodward, Cycloaddition Reactions of Tropone and 2,5-Dimethyl-3,4-diphenylcyclopentadienone. *J. Am. Chem. Soc.* **1970**, *92*, 4145-4147.
22 K. N. Houk, L. J. Luskus, N. S. Bhacca, The Novel [6+4] Cycloaddition of Tropone to Dimethylfulvene. *J. Am. Chem. Soc.* **1970**, *92*, 6392-6394.
23 M. E. Garst, V. A. Roberts, C. Prussin, Steric and Electronic Effects of 1-Substituted Dienes in Cycloaddition Reactions with Cycloheptatrienone. *Tetrahedron* **1983**, *39*, 581-589.
24 J. H. Rigby, T. L. Moore, S. Rege, Synthetic Studies on the Ingenane Diterpenes. Inter- and Intramolecular [6+4] Tropone-Diene Cycloaddition Reactions. *J. Org. Chem.* **1986**, *51*, 2398-2400.
25 L. Isakovic, J. A. Ashenhurst, J. L. Gleason, Application of Lewis Acid Catalyzed Tropone [6+4] Cycloadditions to the

Synthesis of the Core of CP-225,917. *Org. Lett*. **2001**, *3*, 4189-4192.

26 (a) J. H. Rigby, H. S. Ateeq, Synthetic Studies on Transition-Metal-Mediated Higher Order Cycloaddition Reactions: Highly Stereoselective Construction of Substituted Bicyclo[4.4.1]undecane Systems. *J. Am. Chem. Soc.* **1990**, *112*, 6442-6443. (b) J. H. Rigby,N. C. Warshakoon, A. J. Payen, Studies on Chromium(0)-Promoted Higher-Order Cycloaddition-Based Benzannulation. Total Synthesis of (+)-Estradiol. *J. Am. Chem. Soc.* **1999**, *121*, 8237-8245. (c) J. H. Rigby, M. Fleming, Construction of the Ingenane Core using an Fe(III) or Ti(IV) Lewis Acid-Catalyzed Intramolecular [6+4] Cycloaddition. *Tetrahedron Lett.* **2002**, *43*, 8643-8646.

27 R. Mose, G. Preegel, J. Larsen, S. Jakobsen, E. H. Iversen, K. A. Jørgensen, Organocatalytic Stereoselective [8+2] and [6+4] Cycloadditions. *Nat. Chem.* **2017**, *9*, 487-492.

28 A. Patel, Z. Chen, Z. Yang, O. Gutiérrez, H. Liu, K. N. Houk, D. A. Singleton, Dynamically Complex [6+4] and [4+2] Cycloadditions in the Biosynthesis of Spinosyn A. *J. Am. Chem. Soc.* **2016**, *138*, 3631-3634.

29 B. Zhang, K. B. Wang, W. Wang, X. Wang, F. Liu, J. Zhu, J. Shi, L. Y. Li, H. Han, K. Xu, et al. Enzyme-Catalyzed [6+4] Cycloadditions in the Biosynthesis of Natural Products. *Nature* **2019**, *568*, 122-126.

30 C. S. Jamieson, M. Ohashi, F. Liu, Y. Tang, K. N. Houk, The Expanding World of Biosynthetic Pericyclases: Cooperation of Experiment and Theory for Discovery. *Nat. Prod. Rep.* **2019**, *36*, 698-713.

31 P. Caramella, P. Quadrelli, L. Toma, An Unexpected Bispericyclic Transition Structure Leading to 4+2 and 2+4 Cycloadducts in the Endo Dimerization of Cyclopentadiene. *J. Am. Chem. Soc.* **2002**, *124*, 1130-1131.

32 (a) C. Zhou, D. M. Birney, Sequential Transition States and the Valley-Ridge Inflection Point in the Formation of a Semibullvalene. *Org. Lett.* **2002**, *4*, 3279-3282. (b) D. M. Birney, Theory, Experiment and Unusual Features of Potential Energy Surfaces of Pericyclic and Pseudopericyclic Reactions with Sequential Transition Structures. *Curr. Org. Chem.* **2010**, *14*, 1658-1668.

33 B. R. Ussing, C. Hang, D. A. Singleton, Dynamic Effects on the Periselectivity, Rate, Isotope Effects, and Mechanism of Cycloadditions of Ketenes with Cyclopentadiene. *J. Am. Chem. Soc.* **2006**, *128*, 7594-7607.

34 J. B. Thomas, J. R. Waas, M. Harmata, D. A. Singleton, Control Elements in Dynamically Determined Selectivity on a Bifurcating Surface. *J. Am. Chem. Soc.* **2008**, *130*, 14544-14555.

35 D. H. Ess, S. E. Wheeler, R. G. Iafe, L. Xu, N. Çelebi-Ölçüm, K. N. Houk, Bifurcations on Potential Energy Surfaces of Organic Reactions. *Angew. Chem. Int. Ed.* **2008**, *47*, 7592-7601.

36 Z. C. Kramer, B. K. Carpenter, G. S. Ezra, S. Wiggins, Reaction Path Bifurcation in an Electrocyclic Reaction: Ring-Opening of the Cyclopropyl Radical. *J. Phys. Chem. A* **2015**, *119*, 6611-6630.

37 S. R. Hare, R. P. Pemberton, D. J. Tantillo, Navigating Past a Fork in the Road: Carbocation-π Interactions Can Manipulate Dynamic Behavior of Reactions Facing Post-Transition-State Bifurcations. *J. Am. Chem. Soc.* **2017**, *139*, 7485-7493.

38 S. R. Hare, D. J. Tantillo, Post-transition State Bifurcations Gain Momentum – Current State of the Field. *Pure Appl. Chem.* **2017**, *89*, 679-698.

39 P. Yu, T. Q. Chen, Z. Yang, C. Q. He, A. Patel, Y.-H. Lam, C. Y. Liu, K. N. Houk, Mechanisms and Origins of Periselectivity of the Ambimodal [6+4] Cycloadditions of Tropone to Dimethylfulvene. *J. Am. Chem. Soc.* **2017**, *139*, 8251-8258.

40 C. S. Jamieson, A. Sengupta, K. N. Houk, Cycloadditions of Cyclopentadiene and Cycloheptatriene with Tropones: All *Endo*-[6+4] Cycloadditions are Ambimodal. *J. Am. Chem. Soc.* **2021**, *143*, 3918-3926.

41 For a fantastic historical perspective on Diels-Alder reactions and how computational chemistry has impacted our mechanistic understanding of cycloadditions see: K. N. Houk, F. Liu, Z. Yang, J. I. Seeman, Evolution of the Diels-Alder Reaction Mechanism since the 1930s: Woodward, Houk with Woodward, and the Influence of Computational Chemistry on Understanding Cycloadditions. *Angew. Chem. Int. Ed.* **2021**, *60*, 12660-12681.

42 Y. Zhao, D. G. Truhlar, The M06 Suite of Density Functionals for Main Group Thermochemistry, Thermochemical Kinetics, Noncovalent Interactions, Excited States, and Transition Elements: Two New Functionals and Systematic Testing of Four M06-class Functionals and 12 other Functionals. *Theor. Chem. Acc.* **2008**, *120*, 215-241.

43 (a) M. R. Nydenm, G. A. Petersson, Complete Basis Set Correlation Energies. I. The Asymptotic Convergence of Pair Natural Orbital Expansions. *J. Chem. Phys.* **1981**, *75*, 1843-1862. (b) G. A. Petersson, M. A. Al-Laham, A Complete Basis Set Model Chemistry. II. Open-Shell Systems and the Total Energies of the First-Row Atoms. *J. Chem. Phys.* **1991**, *94*, 6081-6090. (c) G. A. Petersson, T. Tensfeldt, J. A. Montgomery, A Complete Basis Set Model Chemistry. III. The Complete Basis Set-Quadratic Configuration Interaction Family of Methods. *J. Chem. Phys.* **1991**, *94*, 6091-6101. (d) J. A. Montgomery, J. W. Ochterski, G. A. Petersson, A Complete Basis Set Model Chemistry. IV. An Improved Atomic Pair Natural Orbital Method. *J. Chem. Phys.* **1994**, *101*, 5900-5909.

44 Z. Yang, X. Dong, Y. Yu, P. Yu, Y. Li, C. Jamieson, K. N. Houk, Relationships Between Product Ratios in Ambimodal Pericyclic Reactions and Bond Lengths in Transition Structures. *J. Am. Chem. Soc.* **2018**, *140*, 3061-3067.

45 J. I. Steinfeld, J. S. Francisco, W. L. Hase, *Chemical Kinetics and Dynamics*, 2nd ed.; Prentice Hall: Upper Saddle River, NJ, 1998.

46 M. J. Frisch, G. W. Trucks, H. B. Schlegel, G. E. Scuseria, M. A. Robb, J. R. Cheeseman, G. Scalmani, V. Barone, G. A. Petersson, H. Nakatsuji, H. et al. *Gaussian 16*, Revision C.01; Gaussian Inc., 2016.

47 Y. Zhao, D. G. Truhlar, Applications and Validations of the Minnesota Density Functionals. *Chem. Phys. Lett.* **2011**, *502*, 1-13.

48 S. Maeda, Y. Harabuchi, Y. Ono, T. Taketsugu, K. Morokuma, Intrinsic Reaction Coordinate: Calculation, Bifurcation, and Automated Search. *Int. J. Quantum Chem.* **2015**, *115*, 258-269.

49 M. Cossi, N. Rega, G. Scalmani, V. Barone, Energies, Structures, and Electronic Properties of Molecules in Solution with the C-PCM Solvation Model. *J. Comp. Chem.* **2003**, *24*, 669-681.

50 CLYview20; C. Y. Legault, Université de Sherbrooke, 2020 (http://www.clyview.org)